

# Experimental setup capable of applying a triaxial state of stress while producing and imaging hydraulic fractures

Gunarathna, G.S.

*New Jersey Institute of Technology, Newark NJ, United States of America*

Gonçalves da Silva, B.

*New Jersey Institute of Technology, Newark NJ, United States of America*

Copyright 2019 ARMA, American Rock Mechanics Association

This paper was prepared for presentation at the 53<sup>rd</sup> US Rock Mechanics/Geomechanics Symposium held in New York, NY, USA, 23–26 June 2019. This paper was selected for presentation at the symposium by an ARMA Technical Program Committee based on a technical and critical review of the paper by a minimum of two technical reviewers. The material, as presented, does not necessarily reflect any position of ARMA, its officers, or members. Electronic reproduction, distribution, or storage of any part of this paper for commercial purposes without the written consent of ARMA is prohibited. Permission to reproduce in print is restricted to an abstract of not more than 200 words; illustrations may not be copied. The abstract must contain conspicuous acknowledgement of where and by whom the paper was presented.

**ABSTRACT:** Hydraulic fracturing can be recognized as an emerging method used in the extraction of oil and gas entrapped within shale formations as well as in the mining of heat in Enhanced Geothermal Systems (EGS). While there are several experimental studies focusing on the initiation and propagation of hydraulically-induced fractures under uniaxial and biaxial loading conditions, a very limited number of experimental studies investigate the effect of triaxial loading conditions on fracture initiation and propagation.

This study describes an experimental setup, which was designed to allow one to independently apply and control three orthogonal stresses in prismatic granite specimens while simultaneously applying a hydraulic pressure inside pre-fabricated flaws. Moreover, the test setup allows one to observe and interpret the fracturing processes through visual and acoustic emission (AE) monitoring. The observations obtained in the current study using a triaxial state of stress were interpreted and compared with existing experimental studies.

It was observed that whitening of some grains and high-amplitude AE events occurred where visible cracks eventually developed for the triaxial state of stress investigated. Comparison with previous studies, in which only vertical loads (uniaxial) were applied, shows that the aperture of the hydraulically induced fractures for the triaxial condition is significantly smaller than for the uniaxial loadings and the coalescence patterns are stress-dependent. In terms of AE data, the total number of AE events in the test under triaxial stresses were significantly higher than in the tests with uniaxial stresses, even though most of the events (65%) had a relatively low-amplitude (<50dB) in contrast to the uniaxial tests, in which low-amplitude events were typically less than 50%.

## 1. INTRODUCTION

Hydraulic fracturing has been widely used in field applications such as in the extraction of shale oil/gas, enhanced geothermal systems (EGS) and also in artificial ground water recharge. Even though hydraulic fracturing has widely been used, the multi-scale fracturing processes involved in it are not entirely understood. Therefore, laboratory experiments [3,5,13,20,22] and numerical analyses [2,6,9,15,18,21,24,25,28] play a key role in understanding the physical mechanisms responsible for the development of hydraulic fractures.

In terms of laboratory experiments, researchers have been looking into the initiation, propagation and eventual coalescence of fractures using various materials with pre-fabricated flaws subjected to uniaxial, biaxial and triaxial states of stress. In 1974, Lajtai [12] used uniaxially-loaded Plaster- of- Paris specimens with a single pre-fabricated flaw to study the crack initiation sequence, observing that tensile cracks are the first to propagate followed by normal and inclined shear cracks.

In 2008, Wong [26] conducted a series of tests on molded gypsum and Carrara marble specimens with single and double pre-fabricated flaw geometries under uniaxial compression. The test setup included a high-speed video camera and a high-resolution camera to clearly distinguish the order of initiation and the nature of the cracks (i.e., tensile, shear, combination of tensile/shear). Bobet [1] observed the fracturing processes in molded gypsum specimens under uniaxial and biaxial loadings. Stoeckert et al. [23] hydraulically fractured Bebertal sandstone specimens subjected to triaxial stresses and Frash et al.[4] successfully used a heated true triaxial apparatus to propagate hydraulic fractures, simulating a binary EGS reservoir created within an intact granite specimen. Researchers have also visually observed the propagation of hydraulic fractures subjected to different vertical stresses; for example, Gonçalves da Silva [7] hydraulically fractured granite specimens with five different pre-fabricated flaw geometries subjected to two vertical loads.

In this study, a test setup is presented that is capable of applying a triaxial state of stress on granite specimens as well as fluid pressure inside pre-fabricated flaws (Fig. 1), with simultaneous visual and acoustic emission monitoring. Initial results obtained in tests that have been recently conducted are also discussed as well as a comparison with existing studies that used different loading conditions. This paper is organized as follows: Section 2 describes the general test setup used in the current study and Section 3 describes the device developed to apply a triaxial load on the specimen and fluid pressure inside the pre-fabricated flaws. Section 4 describes the imaging methods utilized in the tests and the acoustic emission (AE) data acquisition system. Major observations obtained from initial tests (i.e., water pressure variation, image- and acoustic emission analyses) are presented in Section 5 as well as comparisons to existing experimental studies. Finally, Section 6 presents the conclusions reached in this study.

## 2. GENERAL TEST SETUP

The test setup utilized in this study consists of several components (Fig. 2a and 2b) which can be described as follows.

- Pressure enclosure, which encloses the specimen and allows the application of the pressures. There are two connections on the back-steel plate for the application of the fluid pressures: out-of-plane pressure and pressure inside the pre-fabricated flaws.

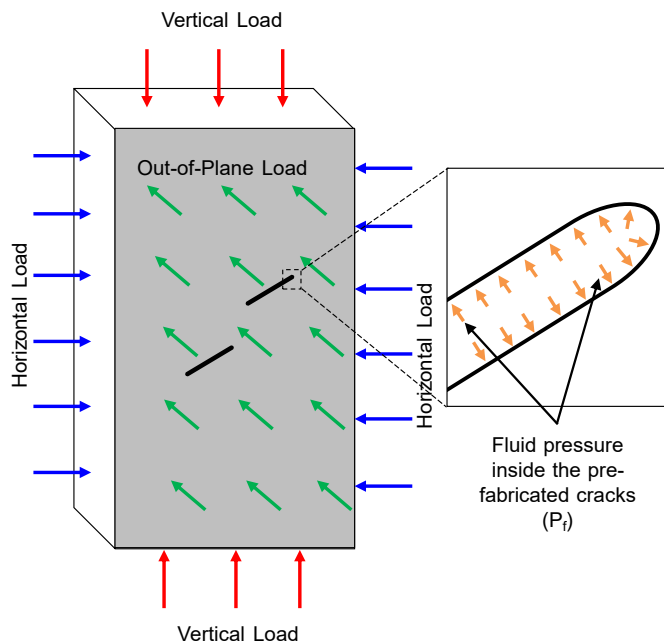


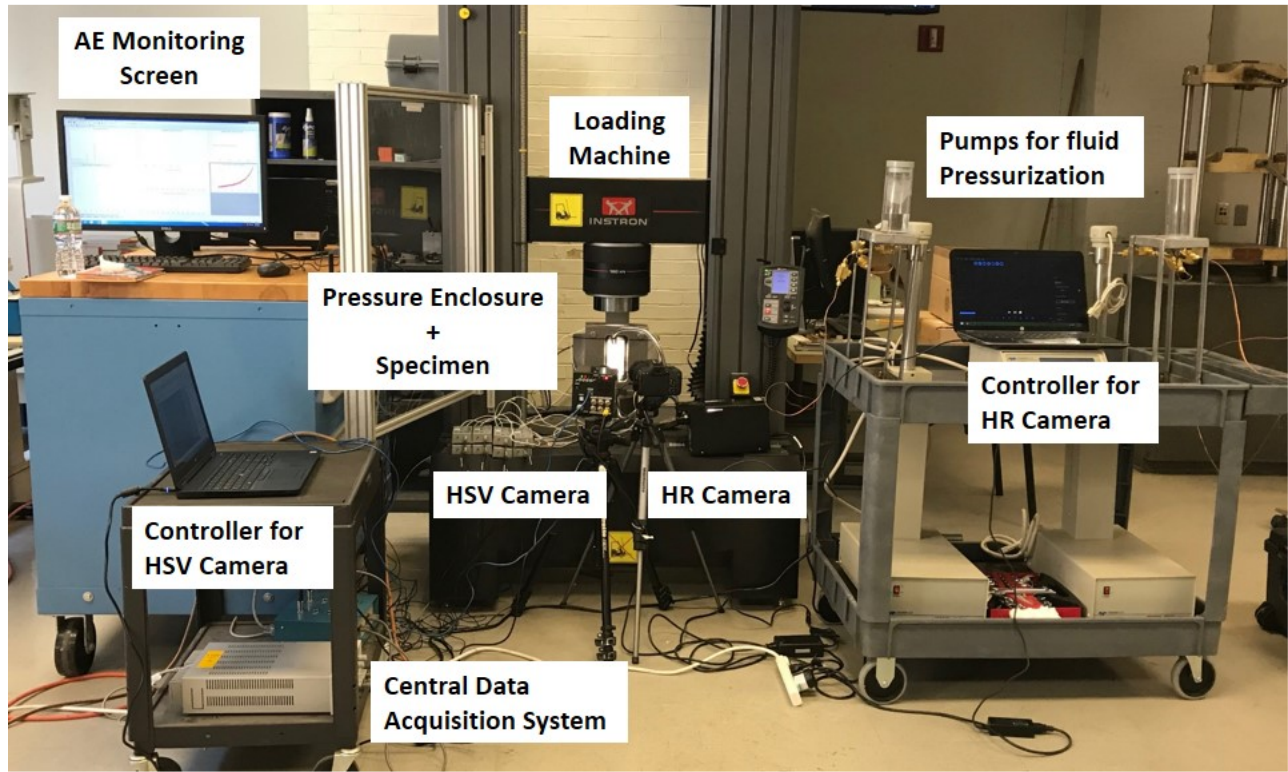
Figure 1. Loading conditions used in this study

- Instron loading machine which applies the vertical load.
- High-speed video (HSV) camera, which records the last few seconds of the test when the specimen breaks. The HSV camera used is a Photron™ Fastcam SA5 with a 90 mm Tamron™ lens. A frame rate of 10,000 per second is usually used in the tests.
- High-resolution (HR) camera. Still frames of the specimen are taken by a HR camera Nikon™ D90 with a 105 mm lens and a 24 Mpixel resolution throughout the test at constant time intervals. It should be noted that the HR camera is the only instrument that is not automatically synchronized with the central data acquisition system, as noted in Fig. 2b.
- Eight wideband differential (WD) acoustic emission (AE) sensors from physical acoustic corporation (PAC) are attached around the specimen in an array. The sensors are connected to pre-amplifiers which, in turn, are connected to the AE data acquisition system. This data acquisition system logs not only the fluid pressures and the trigger time of the HSV camera, but also the waveforms generated by the acoustic emissions produced during the tests. Using only one central data acquisition system has the important advantage of having all these variables synchronized, as illustrated by the dashed lines in Fig. 2b.

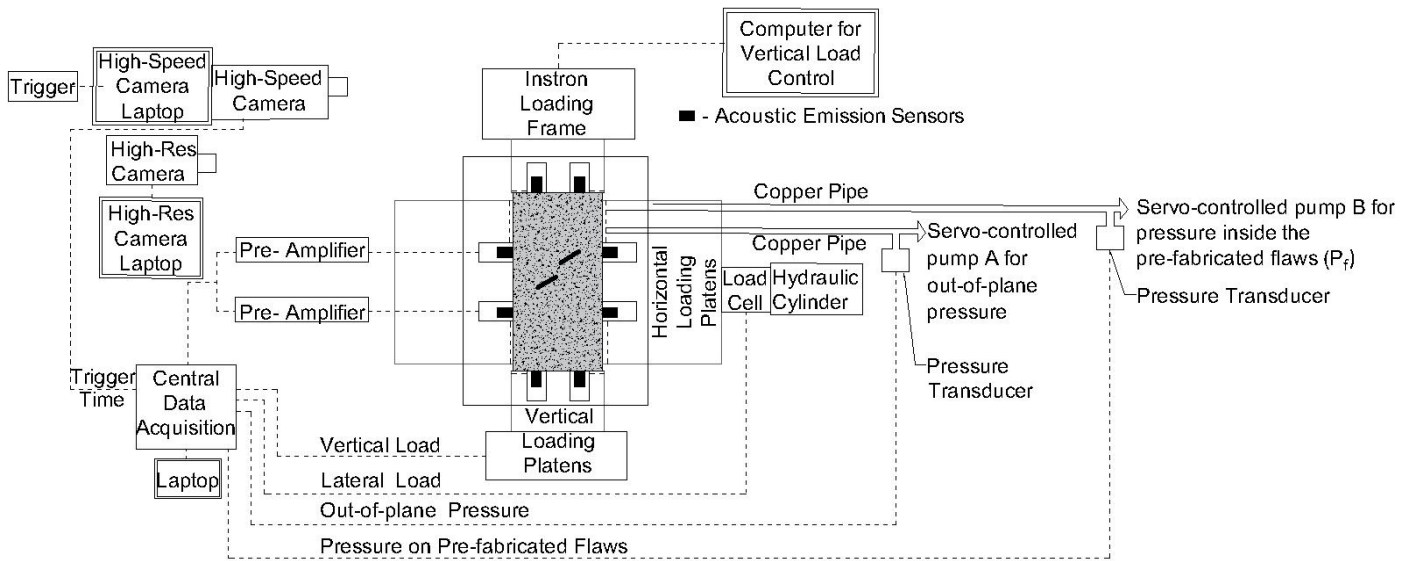
## 3. DEVICE DEVELOPED TO APPLY TRIAXIAL STATE OF STRESS

The new setup is capable of applying an independently controllable triaxial state of stress on the specimen as well as a fluid pressure inside the pre-fabricated flaws. While the vertical load is applied through an Instron loading machine, the remaining loads and pressures are applied with a newly-developed system, which consists of two key parts:

- A pressure enclosure that can apply an out-of-plane pressures and fluid pressures inside the pre-fabricated flaws (Fig. 3)
- A lateral frame which allows one to apply a lateral load to the specimen (Fig. 4)



(a)



(b)

Figure 2. a) Overall view and b) schematic of the test setup used in the hydraulic fracturing tests

Using the newly-designed pressure enclosure, one can simultaneously apply fluid and mechanical pressures to the specimen while monitoring the hydraulic fractures visually and through AE. The enclosure concept was initially developed by Miller [16] and Gonçalves da Silva [7] and alterations were done to separately apply out-of-plane pressures and internal pressures in the pre-fabricated flaws. This device consists of four main components, as illustrated in Fig. 3.

- Two 25.4 mm-thick steel plates on the front and back of the specimen. The front steel plate consists of a window to allow the observation of the fracturing processes. These two steel plates are connected by four bolts. The back-steel plate has two connections for fluid supply, which are connected to TELEDYNE ISCO™ syringe pumps that apply the fluid pressures.
- A 25.4 mm-thick transparent polycarbonate plate between the front steel plate and the granite specimen. The transparent polycarbonate allows the real-time observation of the fracture development while resisting the high fluid pressures reached in the tests.
- Four X-rings; these X-rings have a double sealing capacity as compared to a common O-ring [29] and, therefore require less radial squeeze than an O-ring. This prevents the development of significant stresses near the pre-fabricated flaws due to the friction between the seal and the surface of the specimen. Two of the four X-rings are located between the granite specimen and the polycarbonate plate, and the other two located between the specimen and the back-steel plate. The outer X-ring (Fig. 3a) allows the application of the out-of-plane pressure on the faces of the specimen while the inner X-ring allows one to apply fluid pressure inside the pre-fabricated flaws. The fluid is injected into the specimen from the back-steel plate at a constant injection rate through a servo-controlled injection system (i.e., syringe pumps). It should be noted that only the X-rings are in contact with the rock specimen and not the plates.

Each component of the triaxial loading system was designed to safely reach a fluid pressure of 15MPa.

A schematic of the lateral loading system is shown in Fig. 4. It consists of three A36 steel plates connected by four threaded rods. This system allows the application of a lateral load on the specimen by a 10-ton low-height flat-jack hydraulic cylinder. In addition, eight AE sensor housings were provided in the lateral and vertical platens

to allow one to monitor the AE events throughout the test. Springs were placed inside these housings to press the sensors against the specimen and therefore guarantee good contact between the sensors and the specimen. Figure 5a shows the pressure enclosure and the loading system, as well as the triaxial stresses that can be applied in the experiments. Figure 5b shows the housings provided for the AE sensors.

## 4. IMAGING METHODS AND ACOUSTIC EMISSION DATA ACQUISITION SYSTEM

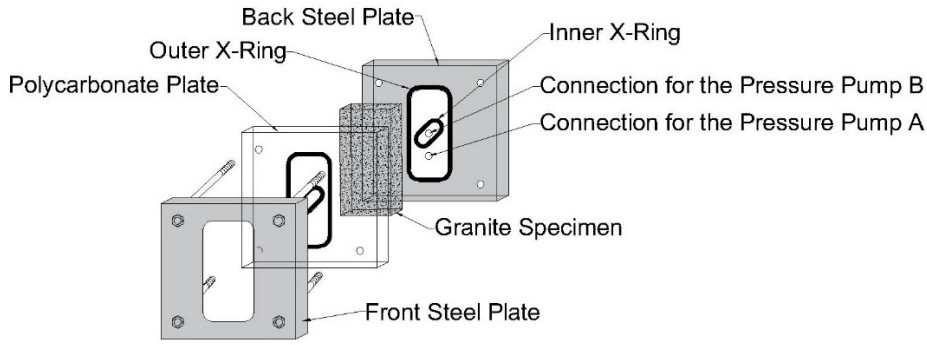
### 4.1. *Imaging Methods*

In laboratory experiments conducted previously, researchers were particularly interested in observing the cracking processes. For example, Wong [26], Gonçalves da Silva [7], Wong & Einstein [27], Morgan et al. [19] used high-resolution (HR) and a high-speed video (HSV) cameras to visualize macro- (i.e. visible with the cameras used) and micro- (i.e. visible as white patches with the cameras used) cracks.

Under this study, two imaging methods are used to capture any occurrence of white patching as well as visible cracks: a HR camera and an HSV camera. The HR camera is set to capture images throughout the test with a rate of 1 frame per second (fps). The HSV camera, on the other hand, captures the last seconds of the test, when the visible cracks develop, with a frame rate of 10,000 fps. During the image analyses, HR images are used to identify white patches and the HSV images are used to recognize the order of visible crack initiation and propagation and the type of cracks produced (tensile, shear or combination of tensile/shear). Specifications of the cameras used are discussed in Section 2. Figure 6 shows typical images obtained using the HR and HSV cameras.

### 4.2. *Acoustic Emission Data Acquisition System*

When a solid crack, it generally releases energy in the form of elastic waves. These elastic waves, which can be treated as acoustic emissions, cause slight movements within the solid that can be detected at its surface [8]. Acoustic emission monitoring plays a significant role in laboratory experiments as a tool to better understand the mechanisms involved in the fracturing of rocks. Ishida [10] monitored the AE events during the hydraulic fracturing of granite using nine cylindrical sensors attached to the upper and lower surfaces of the specimen. Similar studies were also conducted [4,11,13,14,23] to study acoustic emissions generated at the laboratory scale in hydraulic fracturing experiments.



(a)

(b)

Figure 3. a) Scheme of the newly-designed pressure enclosure showing its different parts (b) front view of the pressure enclosure

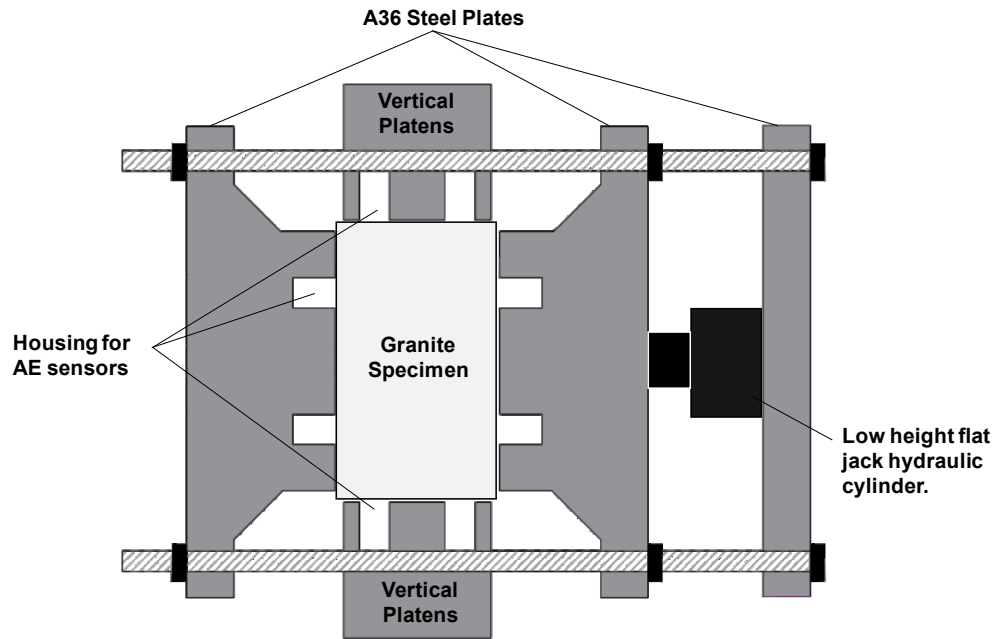
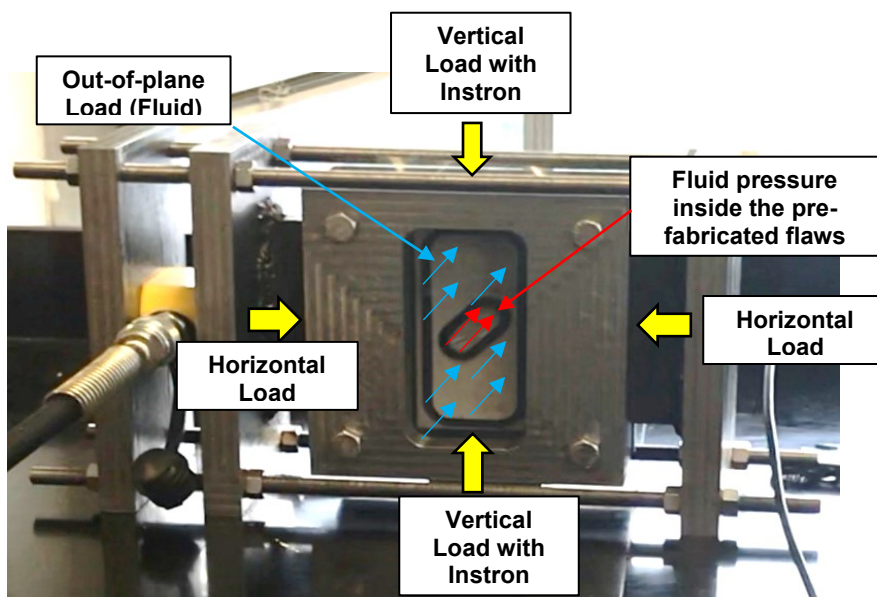


Figure 4. Scheme of the lateral loading system



(a)

(b)

Figure 5. (a) Triaxial loading system (b) housings for the AE sensors

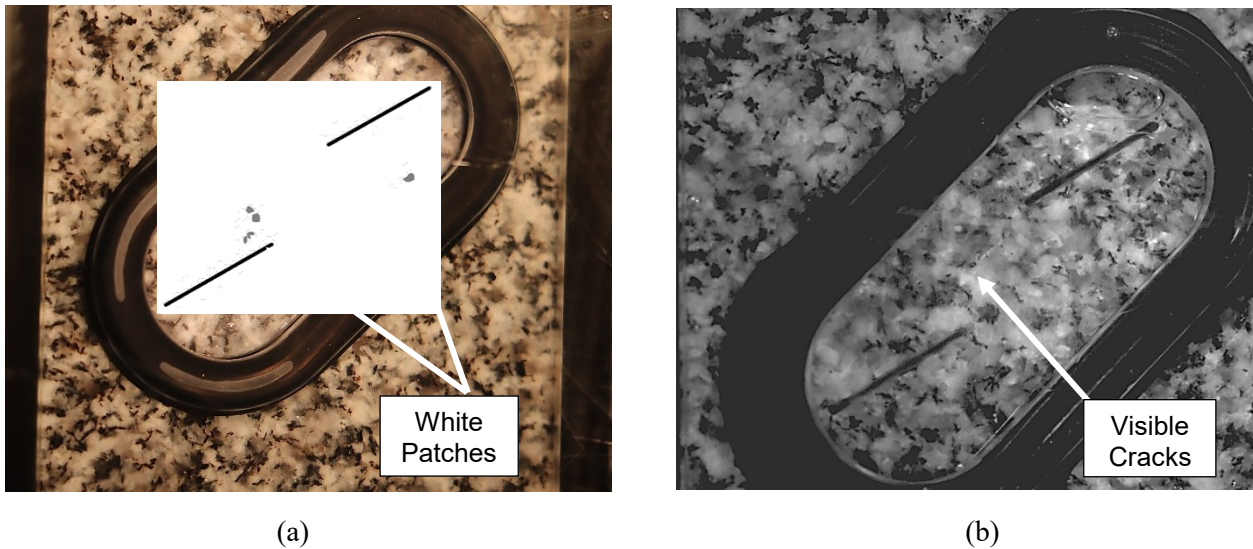


Figure 6. (a) Typical HR frame showing white patching (i.e. micro-damage) identified in the post-test image analysis and (b) HSV frame showing a visible crack. It should be noted that the visible cracks produced under triaxial states of stress are very subtle .

The AE data acquisition system used under this study consist of a Physical Acoustics™ Micro-II Digital AE System, eight wideband differential (WD) sensors and eight pre-amplifiers. The data acquisition system logs the AEs with a sampling rate of 1MHz per channel and the so-called parametric variables (fluid pressures and HSV trigger time) logged with a sampling rate of 100 Hz per channel. The wideband differential sensors have an optimum response frequency in the range of 100-900 kHz [17]. A hit-based method is used to capture the AE signals, in which the system records the wave motion every time a sensor receives a signal with an amplitude above a user-defined threshold (36 dB in the current study).

## 5. INITIAL RESULTS

In this Section, the typical data obtained in a triaxial hydraulic fracturing test with the developed setup will be presented, as well as their interpretation and comparison with existing experiments under different loading conditions in three subsections: in subsection 5.1, the fluid pressure variation observed is discussed, and subsections 5.2 and 5.3 describe the image- and AE data interpretation, respectively.

This Section will focus on the observations and interpretation of the tests performed on granite specimens with a double-flaw geometry of 2a-30-30 subjected to a vertical load, a horizontal load and out-of-plane loads of 4 MPa, 2 MPa and 2 MPa, respectively. It should also be

noted that four tests were conducted for this triaxial loading condition to ensure the repeatability of the tests. The specimens are identified as A,B, C and D in the following Sections. The results obtained with this triaxial state of stress are compared with the observations by Gonçalves da Silva and Einstein [5] for two vertical load conditions: either 5 MPa or 0 MPa.

### 5.1. Fluid Pressure Variation

The hydraulic fracturing tests were conducted at a constant injection rate of 3ml/min. Figure 7 shows the variation of the fluid pressure and the total injected volume for Specimen C. The labels “Sketches 0 to 5” indicate the time and fluid pressure at which the HR and HSV frames and corresponding sketches were taken. This is further explained in Subsection 5.2. It should be noted that Sketches 0-2 are obtained from the analyses of HR camera frames while Sketches 3-5 are obtained from HSV frames. Also, Sketch 0 is captured prior to the application of any fluid pressure inside the pre-fabricated flaws, serving as the baseline to the comparison of images at different stages of the test. For this particular test (Vertical Load = 4MPa; Horizontal Load = 2MPa; Out-of-Plane Pressure = 2MPa) the maximum fluid pressure reached was 8.7 MPa. Figure 8 illustrates the variation of fluid pressure and injected volume with time for the last four seconds of the test. It should be noted that Sketches 3 to 5 are HSV Sketches and Sketches 4 &5 occurred almost simultaneously based on the time scale used.

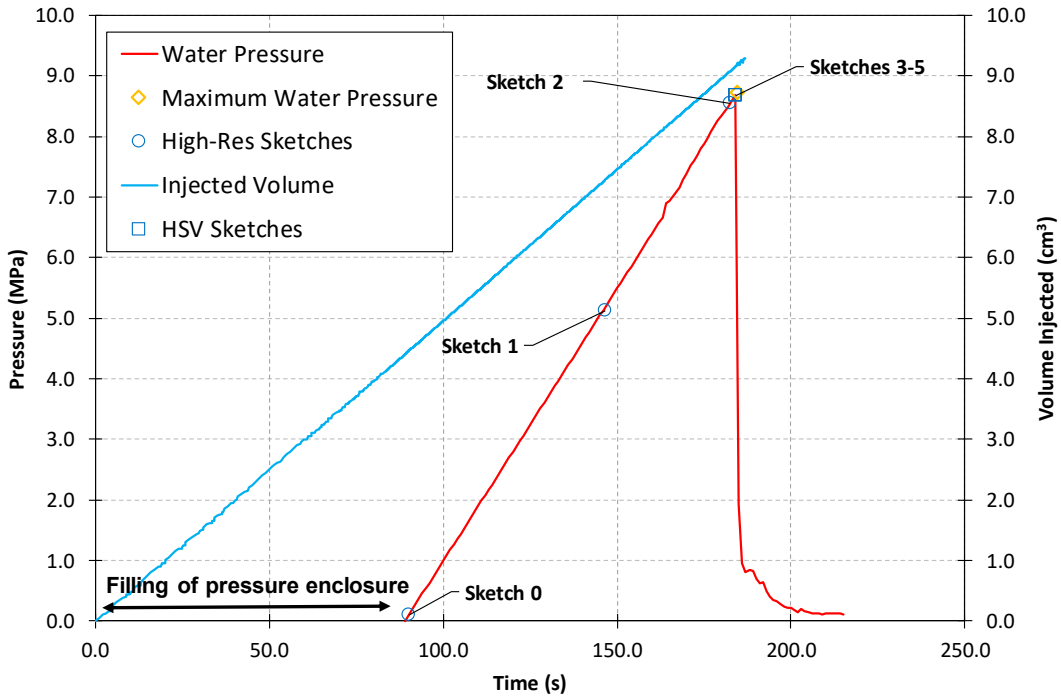


Figure 7. Water pressure and volume of fluid injected vs time for the entire test (Specimen C)

Note: Sketches 0 to 2 obtained from the analyses of HR camera frames and Sketches 3 to 5 were obtained from HSV frames. Sketches 3 to 5 occur almost simultaneously based on the time scale used.

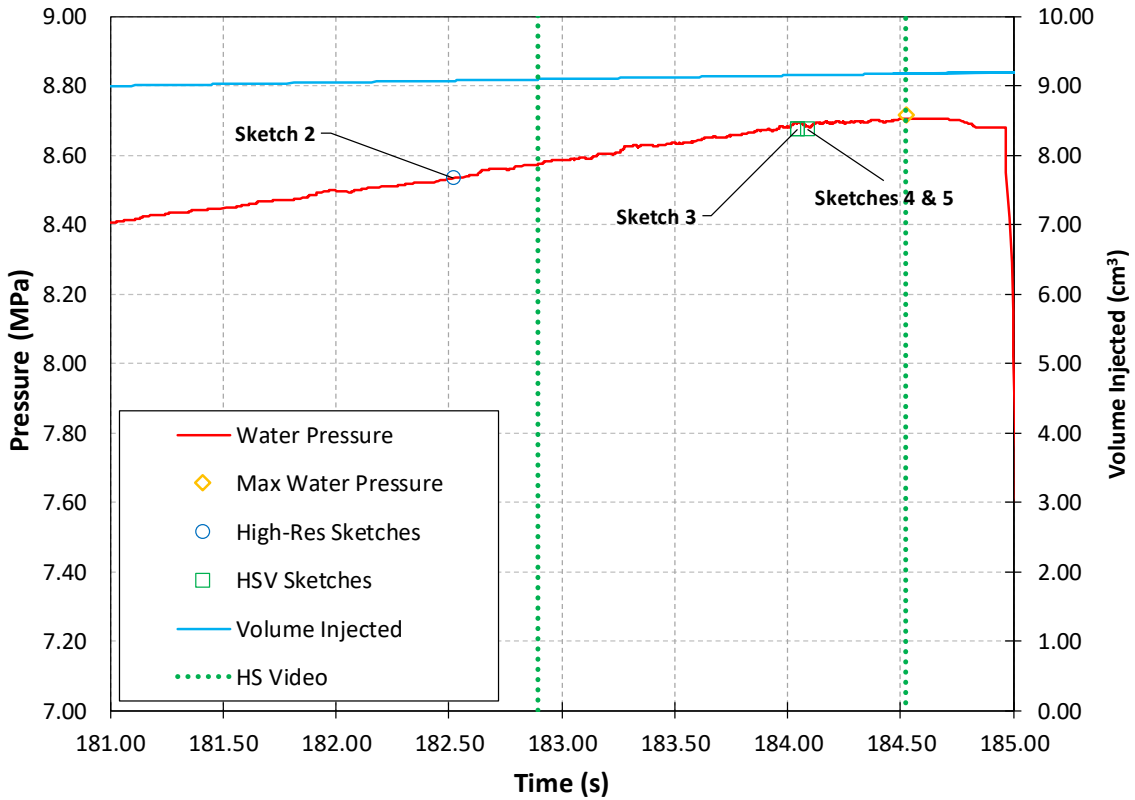


Figure 8. Water pressure and volume of water injected vs time for the last four seconds of the test

Note: Sketches 4 & 5 were obtained with the HSV and occur almost simultaneously based on the time scale used

In order to understand the variation of these breakdown pressures (i.e. in the context of this study, these are the maximum pressures reached in the tests, which typically coincide with visible fracture development), the data obtained from this study is compared with the breakdown pressures observed in the study conducted by Gonçalves da Silva [6]. The study conducted by Gonçalves da Silva [6] investigated the hydraulic fracture propagation under two vertical loading conditions (i.e., Vertical Load = 0MPa, Vertical Load = 5MPa) and five pre-fabricated flaw geometries. For the comparison presented here, only the results obtained for pre-fabricated flaw geometry of 2a-30-30 (the same geometry was tested in the current study) is used. Figure 9 shows the breakdown pressures observed by Gonçalves da Silva [6] and Gonçalves da Silva and Einstein [5] in their experiments for the two vertical loading conditions considered and the breakdown pressures obtained in this study for the triaxial loading condition of Vertical Load = 4 MPa; Horizontal Load = 2 MPa; Out-of-Plane Pressure = 2 MPa. It is clear that the breakdown pressures are considerably higher for the tests conducted with triaxial loading conditions, as intuitively expected.

## 5.2. Image Analysis

For the image analyses, HR and HSV camera frames were analyzed using the software Paint.net. The primary emphasis of these analyses was to investigate the possible initiation of white patches (i.e. micro-damage zone) and visible cracks. Figure 10 shows the analyzed Sketches 1 and 2 (for specimen C) which use HR frames to study the evaluation of white patches before visible cracks develop. Figure 11 shows Sketches 3 and 5 (for specimen C) obtained from HSV camera frames. The evolution of visible cracks occurs rapidly, hence, the HSV frames are used to identify the cracking sequence and type.

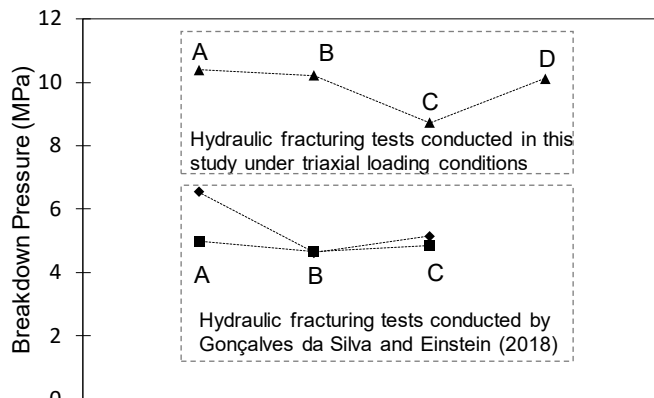


Figure 9. Comparison between the breakdown pressures observed in (a) vertically-loaded specimens by Gonçalves da Silva and Einstein [5] and (b) triaxially loaded specimens under this study

Note: A,B,C,D are the specimens tested for each loading condition.

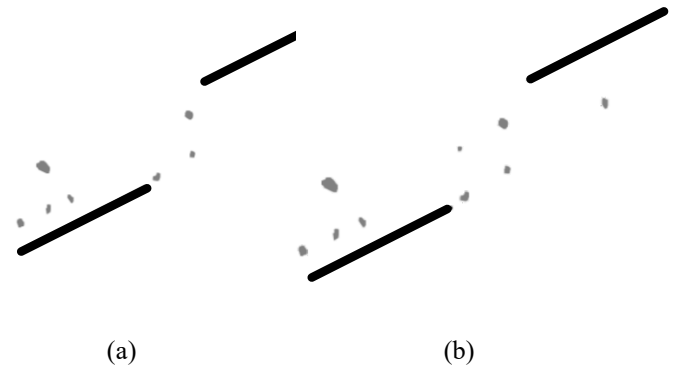


Figure 10. a) Sketch 1 and b) Sketch 2 obtained from the analysis of the HR camera frames, showing the development of white patching for specimen C

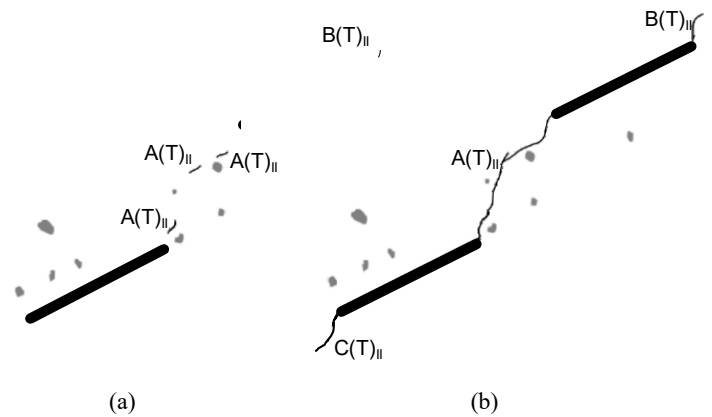


Figure 11. a) Sketch 3 and b) Sketch 5 obtained from the analyses of the HSV camera frames, showing initiation and propagation of visible cracks in specimen C

Note: The letters A, B, C indicate the order of initiation of the cracks, T indicates that the crack is tensile, and the Roman numeral II refers to the type of crack according to Wong and Einstein [17]

Figure 12 shows a comparison between the visible cracks observed during the test analyzed in this study and the hydraulic fracturing tests conducted by Gonçalves da Silva [6] under different vertical load conditions. It is clear that the aperture of the hydraulically-induced fractures for the triaxial loading condition under this study is significantly smaller than for uniaxial loadings. Furthermore, the coalescence patterns are also stress-dependent. As can be seen in Fig. 13(a), the coalescence patterns were vertical load dependent as observed by Gonçalves da Silva Einstein [5]. In the current study, all the specimens tested under the triaxial loading condition with Vertical Load = 4 MPa; Horizontal Load = 2 MPa; Out-of-Plane Pressure = 2 MPa coalesced directly, as shown in Fig.13(b).

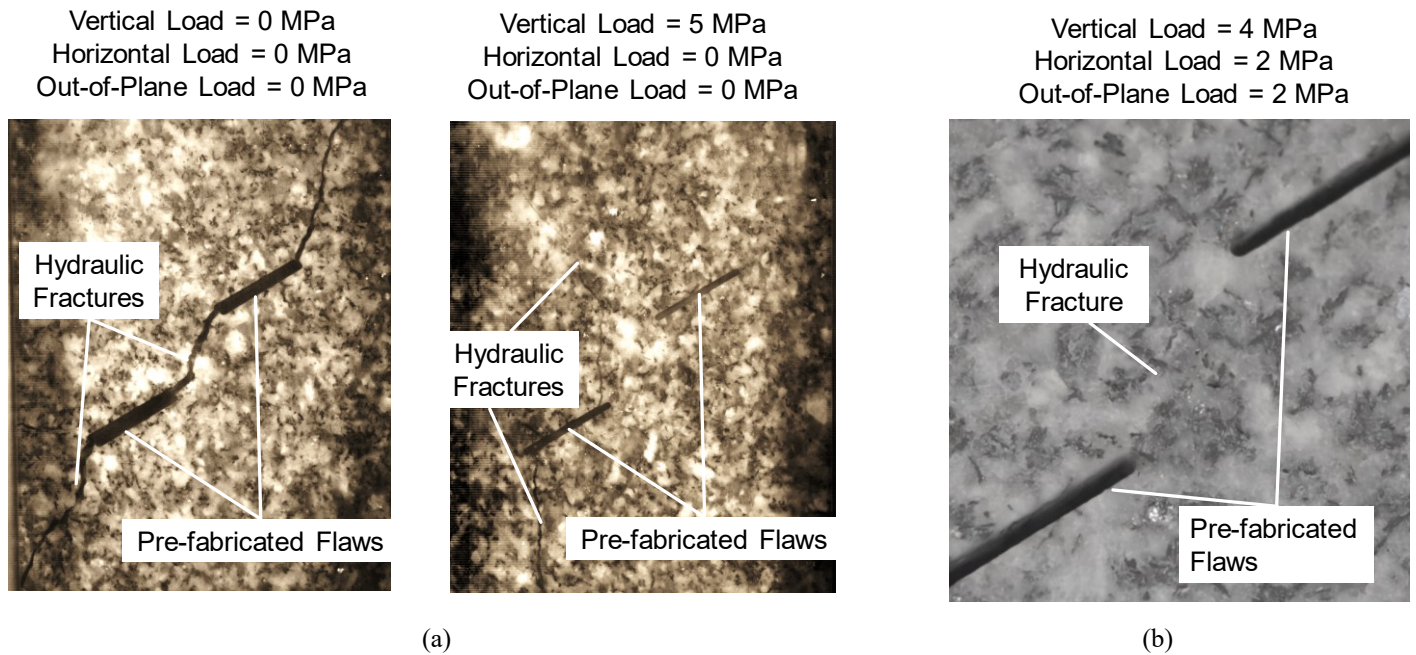


Figure 12. Comparison between the visible hydraulic fractures observed in (a) vertically-loaded specimens by Gonçalves da Silva [6] (b) triaxially loaded specimens under this study

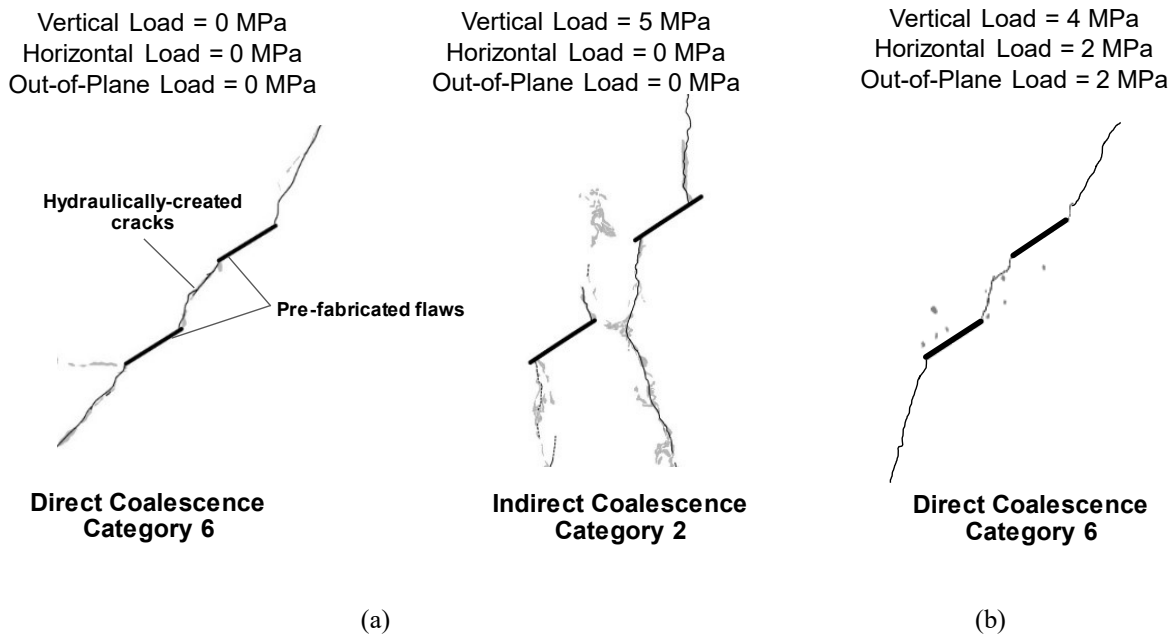


Figure 13. Comparison between the visible hydraulic fractures observed in (a) vertically-loaded specimens by Gonçalves da Silva [6] (b) triaxially loaded specimens under this study

### 5.3. Acoustic Emission Analysis

In the AE analysis, the main variables investigated were (1) the location of the AE events and (2) the amplitude of the first P-wave arrivals. The AE events were categorized according to their first P-wave amplitude (Amplitude < 50 dB, 50dB < Amplitude < 65 dB, Amplitude > 65 dB). This categorization allows one to identify the areas with stronger acoustic activity and to relate them with white patching regions and visible crack development. Figure 14 shows the localization of the AE events captured during the entire test for the Specimen A. The events are predominantly located at or near regions where visible cracks developed, with a particular high-density of events in the bridge between inner flaw tips. Out of the 2399 events recorded, 1735 have amplitudes lower than 50 dB, 566 have amplitudes between 50dB and 65dB and 98 have amplitudes larger than 65dB.

Additionally, a comparison between the number of AE events observed for the vertically-loaded specimens by Gonçalves da Silva [6] and the triaxially-loaded specimens tested under this study is shown in Table 1. The values shown in brackets are the percentage of AE events observed for each amplitude category. Unlike the vertically-loaded specimens, the majority of the AE events (65%) recorded in the triaxially loaded tests have amplitudes lower than 50dB. Overall, it is also clear that the total number of AE events is significantly larger in the tests conducted under triaxial loading conditions.

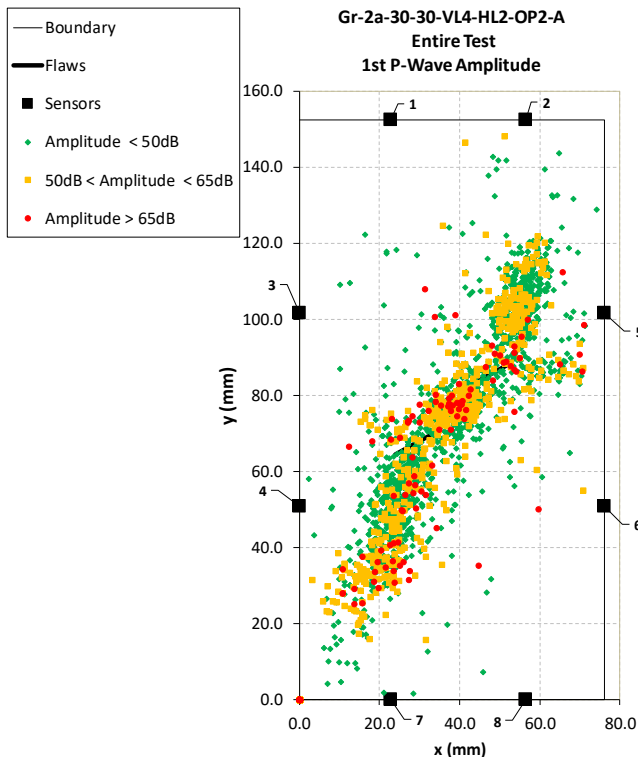


Figure 14. Location of the AE events for Specimen A tested under triaxial conditions in the current study

Moreover, Fig. 15 (a) and (b) shows a comparison between the AE events with amplitude greater than 65 dB recorded for the entire hydraulic fracturing test (Specimen C of both Vertical Load = 0 MPa and Vertical Load = 5 MPa) conducted by Gonçalves da Silva [6] under different vertical load conditions and triaxial loads conducted under this study for specimen C, respectively. Sketch 5, obtained from the image analysis, is also superimposed to the location of the AE events in Fig. 15(b), showing that the events with amplitude larger than 65dB are mainly clustered near the pre-fabricated flaw tips as well as in the bridge region where the visible cracks occur.

### 6. CONCLUSION

This study describes an experimental setup, which was designed to allow one to independently apply and control three orthogonal stresses in prismatic granite specimens while simultaneously applying a hydraulic pressure inside pre-fabricated flaws. Furthermore, the test setup allows one to observe and interpret the fracturing processes through visual and AE monitoring.

The described test setup has been successfully used in a number of hydraulic fracturing tests on granite specimens. The data obtained with the described test setup was shown for a specific triaxial loading condition and the observations were interpreted and compared to existing experiments in which vertical loading conditions were used.

It was noted that the aperture of the hydraulically-induced fractures for the triaxial loading condition under this study is significantly smaller than for the vertical loading and that the coalescence patterns observed are stress-dependent. In addition to that, it was clear that breakdown pressures are considerably higher in the triaxially-loaded specimens. In terms of AE data obtained, it was clear that the total number of AE events is significantly larger for the tests conducted under triaxial loading conditions and that most of the AE events have amplitude lower than 50dB, in contrast to what was observed in the vertically-loaded experiments, in which only a minority of AE had amplitudes lower than 50 dB.

### Acknowledgment

The authors would like to express their gratitude for the support from NSF, through award number 1738081, under which the present study was conducted.

Table 1. Number of AE events for tests conducted on vertically-loaded specimens by Gonçalves da Silva [6] and triaxially-loaded specimens under this study

Loading Condition		Number of Events		
		Amplitude < 50dB	50dB < Amplitude < 65dB	Amplitude > 65dB
Vertically-loaded	Vertical Load = 0 MPa	102 (26.2%)	211 (54.2%)	76 (19.6%)
	Vertical Load = 5 MPa	51 (17.5%)	118 (40.4%)	123 (42.1%)
Triaxially-loaded	Vertical Load = 4MPa Horizontal Load = 2MPa Out-of-Plane Pressure=2MPa	1494 (65.0%)	633 (27.5%)	172 (7.5%)

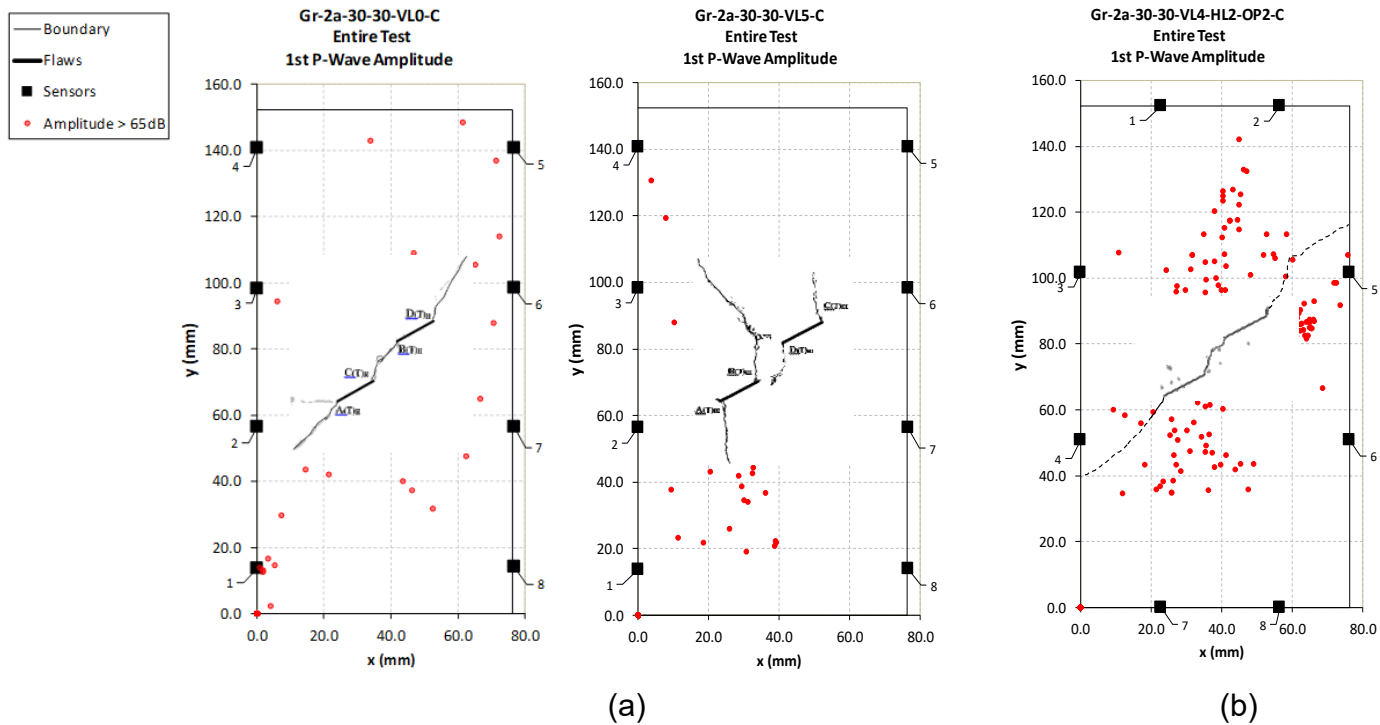


Figure 15. Comparison between the location of AE events with first P-wave amplitude > 65dB for the entire test in (a) vertically-loaded specimens by Gonçalves da Silva [6] and (b) triaxially loaded specimens under this study

## REFERENCES

- [1] A. Bobet, H.H. Einstein, Fracture coalescence in rock-type materials under uniaxial and biaxial compression, *Int. J. Rock Mech. Min. Sci.* 35 (1998) 863–888.
- [2] A. Dahi-Taleghani, J.E. Olson, Numerical Modeling of Multistranded-Hydraulic-Fracture Propagation: Accounting for the Interaction Between Induced and Natural Fractures, *SPE J.* 16 (2011) 575–581.
- [3] L. Frash, Laboratory-scale study of hydraulic fracturing in heterogeneous media for enhanced geothermal systems and general well stimulation (Ph.D Thesis), Civil and Environmental Engineering, Colorado School of Mines, 2007.
- [4] L.P. Frash, M. Gutierrez, J. Hampton, True-triaxial apparatus for simulation of hydraulically fractured multi-borehole hot dry rock reservoirs, *Int. J. Rock Mech. Min. Sci.* 70 (2014) 496–506.
- [5] B. Gonçalves da Silva, H. Einstein, Physical processes involved in the laboratory hydraulic fracturing of granite: Visual observations and interpretation, *Eng. Fract. Mech.* 191 (2018) 125–142.
- [6] B. Gonçalves da Silva, H.H. Einstein, Finite Element study of fracture initiation in flaws subject to internal fluid pressure and vertical stress, *Int. J. Solids Struct.* 51 (2014) 4122–4136.
- [7] B.G. Gonçalves da Silva, Fracturing processes and induced seismicity due to the hydraulic fracturing of rocks (Ph.D Thesis), Massachusetts Institute of Technology, 2016.
- [8] C.U. Grosse, Acoustic Emission Testing Basics for Research - Applications in Civil Engineering, in: C. Ohtsu, G. Masayasu (Eds.), Springer-Verlag Berlin and Heidelberg GmbH & Co. K, 2008.
- [9] G.S. Gunarathna, B. Gonçalves da Silva, Finite Element Study of the Stress Field Near Pressurized and Non-Pressurized Flaws in Rock Specimens Subject to Uniaxial and Biaxial Loads, 52nd U.S. Rock Mech. Symp. (2018) 19.
- [10] T. Ishida, Acoustic emission monitoring of hydraulic fracturing in laboratory and field, *Constr. Build. Mater.* 15 (2001) 283–295.
- [11] T. Ishida, K. Aoyagi, T. Niwa, Y. Chen, S. Murata, Q. Chen, Y. Nakayama, Acoustic emission monitoring of hydraulic fracturing laboratory experiment with supercritical and liquid CO<sub>2</sub>, *Geophys. Res. Lett.* 39 (2012) 1–6.
- [12] E.Z. Lajtai, Brittle fracture in compression, *Int. J. Fract.* 10 (1974) 525–536.
- [13] B.Q. Li, Z. Moradian, B. Gonçalves Da Silva, J.T. Germaine, Observations of acoustic emissions in a hydraulically loaded granite specimen, 49th US Rock Mech. / Geomech. Symp. 2015. 3 (2015).
- [14] Q.B. Li, Acoustic Emissions in Hydraulic Fracturing of Barre Granite (MS.c Thesis), Massachusetts Institute of Technology, 2013.
- [15] M.W. McClure, Modeling and Characterization of Hydraulic Stimulation and Induced Seismicity in Geothermal and Shale Gas Reservoirs (Ph.D Thesis), Stanford University, 2012.
- [16] J.. Miller, Crack coalescence in Granite (MS.c Thesis), Massachusetts Institute of Technology, 2008.
- [17] MISTRAS Group Inc., Express-8 AE System User's Manual, New Jersey, 2014.
- [18] N. Moës, J. Dolbow, T. Belytschko, A finite element method for crack growth without remeshing, *Int. J. Numer. Methods Eng.* 46 (1999) 131–150.
- [19] S.P. Morgan, C.A. Johnson, H.H. Einstein, Cracking processes in Barre granite: fracture process zones and crack coalescence, *Int. J. Fract.* 180 (2013) 177–204.
- [20] S.P. Morgan, B.Q. Li, H.H. Einstein, Effect of Injection Rate on Hydraulic Fracturing of Opalinus Clay Shale, in: 51st U.S. Rock Mech. Symp., 2017.
- [21] M. Nikolić, T. Roje-bonacci, A. Ibrahimbegović, Overview of the numerical methods for the modelling of rock mechanics problems, *Teh. Vjesn. - Tech. Gaz.* 23 (2016) 627–637.
- [22] P.H. Solberg, D. Lockner, J.D. Byerlee, Hydraulic Fracturing in Westerly Granite Under Geothermal Conditions, *Int. J. Rock Mech. Min. Sci.* 3 (1979) 163.
- [23] F. Stoeckhert, M. Molenda, S. Brenne, M. Alber, Fracture propagation in sandstone and slate e Laboratory experiments , acoustic emissions and fracture mechanics, *J. Rock Mech. Geotech. Eng.* 7 (2014) 237–249.
- [24] C. Tang, Numerical simulation of progressive rock failure and associated seismicity, *Int. J. Rock Mech. Min. Sci.* 34 (1997) 249–261.
- [25] M. Vahab, S. Akhondzadeh, A.R. Khoei, N. Khalili, An X-FEM investigation of hydro-

fracture evolution in naturally-layered domains,  
Eng. Fract. Mech. 191 (2018) 187–204.

- [26] L.N.Y. Wong, Crack Coalescence in Molded Gypsum and Carrara Marble (Ph.D Thesis), Massachusetts Institute of Technology, 2008.
- [27] L.N.Y. Wong, H.H. Einstein, Crack Coalescence in Molded Gypsum and Carrara Marble: Part 2—Microscopic Observations and Interpretation, Rock Mech. Rock Eng. 42 (2009) 513–545.
- [28] L.N.Y. Wong, H.Q. Li, Numerical study on coalescence of two pre-existing coplanar flaws in rock, Int. J. Solids Struct. 50 (2013) 3685–3706.
- [29] X-Rings Overview, Glob. O-Ring Seal. (n.d.).